**ACTA ACUSTICA UNITED WITH ACUSTICA**
**Vol. 93 (2007) 314 – 323**

# Experimental Validation of Some Issues in Lip and Vocal Fold Physical Models

A. Van Hirtum, J. Cisonni, N. Ruty, X. Pelorson
Institut de la Communication Parlée, UMR CNRS 5009, INPG-Université Stendhal, 46 Av. Félix Viallet, 38031 Grenoble, France. pelorson@icp.inpg.fr

I. Lopez, F. van Uittert
Eindhoven University of Technology, Postbus 513, 5600 MB Eindhoven, The Netherlands

*Invited paper based on a presentation at Forum Acusticum 2005 in Budapest*

**Summary**
Insight into vocal fold and lip oscillation mechanisms is important for the understanding of phonation and the sound generation process in brass musical instruments. In general, a simplified analysis of the physical 3D fluid-structure interaction process between the living tissues and the airflow is favoured by most workers. Several simple models (lumped parameter models) have been proposed and these represent the tissues as a distribution of elastic mass(es). The mass-spring-damper system is acted on by a driving force resulting from the pressure exerted by the airstream. The results from these theoretical models have been validated 'in-vitro' using rigid or deformable replicas mounted in a suitable experimental set-up. Previous research by the authors focused on the prediction of the pressure threshold and oscillation frequency of an 'in-vitro' replica, in the absence and presence of acoustical feedback. In the theoretical model a lip or vocal fold is represented as a simple lumped mass system. The model yielded accurate prediction of the oscillation threshold and frequency. In this paper a new 'in-vitro' set-up is presented, which overcomes some of the limitations of the previous study. By the use of a digital camera synchronised with a light source and of pressure sensors, this set-up allows 1) measurement of the area of the replica opening and 2) imposition of independent initial conditions, such as height of the initial opening and internal pressure in the replica. The impact of these findings on physical modelling is discussed.

**PACS no. 43.70.Jt, 43.70.Bk, 43.75.Fg**

## 1. Introduction

Physical vocal fold and lip models are used to predict the oscillatory behaviour of tissue in terms of the relevant physical quantities. These include the minimum pulmonary or mouth pressure $P_{thres}$ necessary to sustain oscillation, the oscillation frequency $F_0$, the tissue geometry and mechanical tissue properties. Recent publications on physical modelling involve the application of complex numerical [1, 2, 3] as well as simplified theoretical models [4, 5, 6, 7, 8]. Simplified theoretical models, such as lumped parameter models, aim to mimic the ongoing physiological fluid-structure interaction with a limited number of model parameters. Interpretation of 'in-vivo' observations in terms of model input parameters and in terms of the model output is severely hampered by the complexity of the fluid-structure interaction. The difficult or only indirect access to the mechanical properties of the lips and of the vocal folds of living subjects during instrument playing or phonation, also presents severe problems. Therefore, validation of theoretical models in terms of accuracy, reproducibility and sensitivity to variation of an individual parameter is performed on mechanical replicas in combination with a suitable experimental set-up. In addition, the use of an experimental set-up makes it possible to focus on the modelling of specific physical issues involved in the oscillatory cycle. These include acoustical feedback or tissue collision which can hardly be attempted 'in-vivo', since 'in-vivo' phonation presents itself as an indivisible entity which cannot be split up into distinct separable and controllable events. So although 'in-vivo' observations are extremely important as a benchmark for the phenomena under study, mechanical replicas with increasing degrees of complexity are developed in order to study physical models [9, 4, 10, 11, 12, 13, 14]. In [15, 16], a deformable 'in-vitro' replica and experimental set-up is presented in order to validate low-order one or two-mass physical models. These low-order models yielded accurate predictions of the minimum pressure required to retrieve the oscillation onset $P_{thres}$ and the oscillation frequency $F_0$ in the presence and absence of acoustical feedback. In this paper, some improvements in the deformable replica and experimental set-up described in [4, 15, 16] are presented

Received 10 February 2006,
accepted 22 September 2006.

in order to improve accuracy with the set of model input parameters. Since the tissue oscillation is a highly non-linear phenomenon it is likely to be dependent on initial conditions [17]. Therefore, and in order to explore the parameter space, the replica is modified so that distinct initial conditions, like the initial opening at rest, can be imposed independently. Next, the experimental set-up is elaborated in order to allow the open area of the replica to be measured directly instead of being estimated from the centre height of the replica aperture. Current research in musical acoustics is attempting to refine the general function relating the centre height of the aperture and the open area between the lips and to study the impact on the sound output characteristics of a brass instrument model [14, 18]. In this study, validation of low-order physical vocal fold models, accounting for a more accurate open area measurement, is carried out. This is achieved without attempting to redefine the functional relationship, which is assessed in terms of the physical quantities predicted in [4, 15, 16], i.e. the pressure associated with oscillation onset $P_{thres}$ and the corresponding oscillation frequency $F_0$.

## 2. 'In-vitro' set-up

In the following section, modifications to the deformable replica and to the experimental set-up described in [4, 19, 16] are presented. The resulting replica is illustrated in Figure 1.

### 2.1. Deformable vocal folds or lips replica

In the same way as for the deformable replica assessed in [4, 19, 15, 16], the vocal folds or lips are mimicked by two connected latex tubes (Piercan Ltd) of 12 mm diameter and 0.3 mm wall thickness. The tubes are mounted on two metal cylinders with diameter 12 mm, for which the metal is removed over half the diameter for a length of 40 mm, labelled part [a] in Figure 1a. The latex tubes are filled with water supplied through a central duct of 3 mm diameter connected to a water column, indicated as part [c] in Figure 1a. The height of the water column is controllable. In this way the internal pressure $P_{in}$ in the latex tubes is also controllable. The latex tubes are positioned in a metal block corresponding to parts [b,b'] in Figure 1a, in order to prevent leakage. In the previous replica the metal block was a fixed entity so that the latex tubes could only be placed in one way. Obviously increasing or decreasing the internal pressure $P_{in}$, by lifting or lowering the water column, was the only way of altering the initial aperture between the two tubes. Consequently the internal pressure $P_{in}$ in the latex tubes and the initial aperture $h_0$ were not independent quantities. Because of the non-linear nature of the oscillatory behaviour and hence the importance of the initial conditions, this was a severe limitation of the previous study. Besides, the reciprocal dependence also restricted the range of experimentally accessible ($P_{in}$,$h_0$)-values in the parameter space. In order to enable independent variation of $P_{in}$ and $h_0$, the mounting position of the tubes can be varied by means of the fixing screws indicated in Figure 1a as [e]. Besides the fixing screws, separators of a suitable height [d',d] are placed between the latex tubes at the outer borders in order to prevent leakage. The screws and separators allow $h_0$ to vary from complete closure, $h_0 = 0$ (see Figure 1c and [d'] in Figure 1a), to a maximum opening of $h_0 = 10$ mm (see Figure 1b and [d] in Figure 1a). In the present work, separators of height 0.0, 0.5 and 1.0 mm are used in order to significantly vary the initial aperture of the replica and to experimentally explore a considerable region in the independent ($P_{in}$,$h_0$)-parameter space.

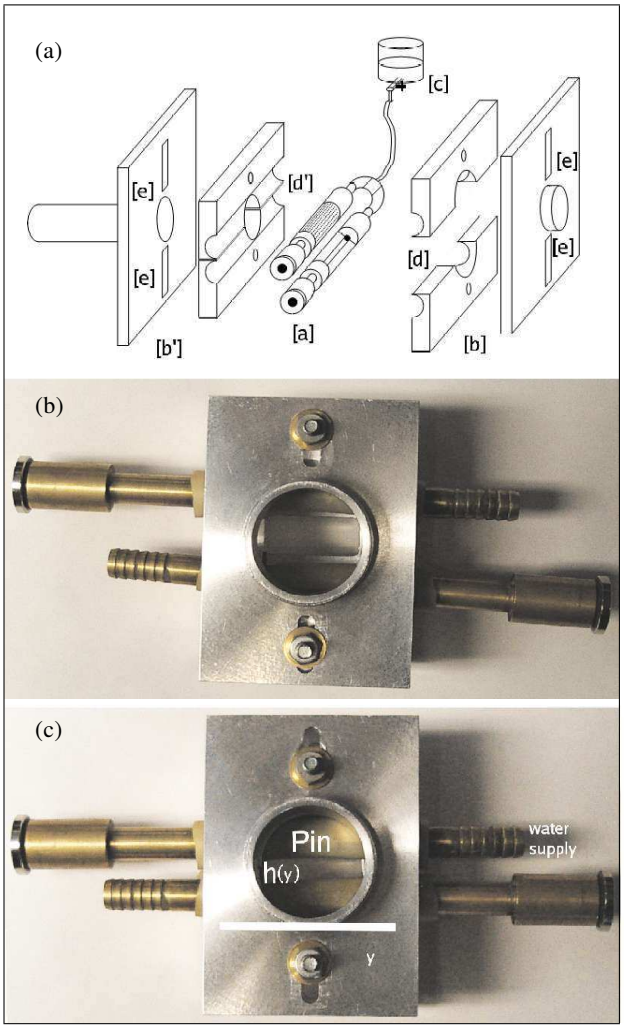


Figure 1. Mechanical vocal fold replica with fixing screws and separators, allowing the variation of the initial aperture $h_0$: (a) schematic view and (b) photo showing maximum $h_0 = 10$ mm, and (c) minimum $h_0 = 0$ mm. In part (a), [a] indicates the latex tubes connected to a water column [c] to impose $P_{in}$. The latex tubes are mounted in a metal block by means of fixing screws [e]. The initial aperture between the tubes is variable by placing separators [d] between the outer parts of the upper and lower portion of the mounting block. In the absence of separators [d'] the aperture is minimal.

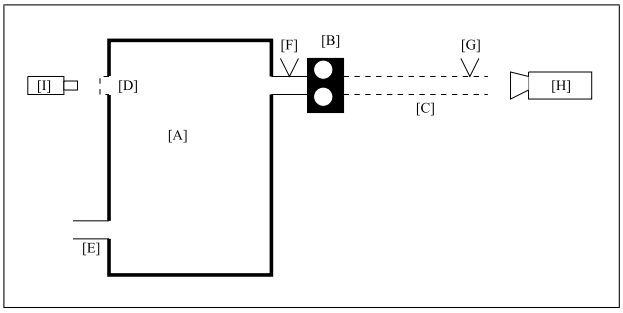


Figure 2. Schematic representation of the visualisation/optical setup: [A] pressure tank, [B] replica, [C] downstream waveguide, [D] transparent window, [E] air supply, [F] upstream pressure tap $P_{up}$, [G] downstream pressure tap $P_d$, [H] camera/diode, [I] flashlamp/laser.

### 2.2. Experimental set-up with deformation visualisation

#### 2.2.1. Air supply and pressure measurements

The experimental set-up was inspired by the set-up presented in [4, 19, 16]. The existing set-up is extended in order to improve visualisation of the deformation of the mechanical replica during the fluid-structure interaction. A schematic representation of the set-up is given in Figure 2. As in previous work, an air supply [E] is connected to a pressure tank of 0.75 $m^3$ filled with acoustical foam [A], enabling imposition of an airflow through the deformable replica [B]. The pressure upstream from the replica, $P_{up}$, can be measured by means of a dynamic piezo-resistive pressure transducer (Endevco 8507C or Kulite XCS-093) positioned in a pressure tap [F] of 0.4 mm diameter. In the same way the downstream pressure, $P_d$, can be measured at a pressure tap [G] when a downstream pipe [C] is attached to the replica. The pressure transducers are calibrated against a water manometer with an accuracy of 1 Pa. The attached circular pipes have an internal diameter of 25 mm and length, $L$.

#### 2.2.2. Deformation visualization with laser

Previously, the frequency response, the geometry and the deformation of the replica were observed by means of a laser beam (635 nm) passing through the replica and brought to focus on a light sensitive diode (BPW 34) [16]. In Figure 2 the laser device is indicated by [I]. The beam passes through a transparent window [D], through the replica and the transmitted portion of the beam intensity is measured by means of a diode [H]. The width of the laser beam covers only a limited part of the width of the open area, $A$, between the two replica tubes. Therefore, the optical laser system was calibrated to relate the transmitted light intensity of the original beam to the centre height ($h_c$) between the two tubes at the centre of the open area. In this way time-varying centre heights $h_c(t)$ up to 6 mm can be measured with an accuracy of 0.01 mm. The measured height $h_c(t)$ was related to the open area $A_c(t)$ by assuming parallel tubes or a rectangular open area, i.e. $A_c(t) = h_c(t)w$ with $w = 25$ mm being the constant width of the replica exposed to the airflow.

#### 2.2.3. Camera-based visualization system

Experimental research on lip or vocal fold replicas has shown that the assumption of a rectangular opening area to be inaccurate [16, 14]. Consequently, the estimation of the volume flow, $U(t)$ applied in the fluid model is also inaccurate. In order to increase the accuracy of the open area estimation, the optical laser system was replaced in this study by an image acquisition system capable of visualising the open area between the latex tubes during the fluid structure interaction. The visualisation set-up is again schematically represented by Figure 2, but part [I] represents a flashlight (FX1101, BFiOPTiLAS) or ordinary light source, and [H] a digital camera (Inca311 with resolution 1280x1024 pixels, Philips). The settings of the camera and zoom objective were adjusted in order to maximise the number of pixels occupied by the open area between the replica tubes. So the images are less than 1280x1024 data matrices with grey values varying from 0 (black) to 255 (white). A standard three-step image analysis procedure, consisting of image segmentation, erosion and dilatation is applied to the data matrices in order to produce binary images of the open area [20]. In order to relate the obtained open area in pixels to the requested value in $mm^2$, a calibration of the 2D-images is performed. The horizontal and vertical resolutions of $\Delta w$ and $\Delta h$, respectively, for the spatial sampling yields about $6 * 10^{-3}$ cm/pixel. So an error rate of one pixel corresponds to an error of about 0.06 mm along both the horizontal and vertical axes. The area values are obtained from the processed images. Assuming a rectangular area function, the area $A$ is given as $A = w.h$, where $h$ denotes the aperture and $w = 25$ mm the fixed width. The area error $\Delta A$ ,which is a function of the spatial sampling rate, is derived as $\Delta A = \sqrt{w^2(\Delta h)^2 + h^2(\Delta w)^2}$. The relative error $\Delta A/A$ increases with decreasing $h$, e.g. for $h = 1$ and 3 mm the relative error yields 6% and 2%, respectively.

The camera and the flashlight are triggered with respect to the upstream pressure $P_{up}$ in order to acquire images of the open area $A$ at different stages during the fluid-structure interaction. This enables visualisation of different degrees of deformation and hence variations of the original open area $A^0$. More particularly, a step-trigger is applied where $P_{up}$ is gradually increased (between 0 and $\pm$2500 Pa) and an image is acquired whenever $P_{up}$ is raised with a fixed step of 50 Pa. In the following discussion, the (y,z)-plane is defined as the visualised plane containing the open area, with the y-axis parallel to the mid-line between the latex tubes and the z-axis in the direction of the open area height, perpendicular to the mid-line. The x-axis is pointing in the direction of incoming airflow.

## 3. Physical modelling

In [4, 15, 16] physical modelling of the self-sustained oscillations of the replica was performed by applying theoretical one- and two-mass physical models and exploiting the relationship between the input and output parameters in the physical model and the measured experimental vari-

ables. Briefly, the replica is modelled as a reduced spring-mass-damper system with one of two degrees of freedom driven by the pressure difference across the masses. The oscillation frequency $F_0$ and the minimum upstream pressure $P_{thres}$ required to maintain the oscillation are derived by linearising the physical quantities and assuming only small variations occur around the equilibrium position. This assumption is motivated by the desire to make predictions regarding the onset of self-sustained oscillations. The required values of $F_0$ and $P_{thres}$ are easily retrieved from the eigenvalues of the state space matrix of the linearised system by looking at the sign of their real part. Linear stability analysis of the one-(delayed)-mass and two-mass model are briefly described in subsections 3.1 and 3.2 and the model input parameters are outlined. In [15, 16] a procedure is established in order to relate experimental control parameters to the required model parameters. Besides the measurement of the upstream $P_{up}$ and downstream $P_d$ pressure, the mechanical model parameters related to the spring and damper variables are obtained from measurements of the mechanical response of the replica. Finally, the initial aperture distance $\overline{H}$ between the latex tubes at equilibrium needs to be experimentally estimated, since the mechanical model assumes a rectangular open area $A$ of fixed width $w$=25 mm. The experimental parameters and the features derived from open area imaging are further discussed in section 4. The next subsections briefly discuss the applied one-(delayed)-mass and two-mass models.

### 3.1. One-delayed-mass model and linear stability analysis

The one-delayed-mass model proposed in [5] is an extension of the classical one-mass model [4] and can be seen as a major simplification of the distributed two-mass model [21, 8]. The one-delayed-mass model assumes that the vocal fold motion can be described as a two-mass motion, but where the motion of the second mass is identical to the motion of the first mass except for a fixed time-delay $t_0$. Hence, the mechanical motion is fully determined by the motion of the first mass, and the value of the parameter $t_0$ defines the fixed phase relationship between the two masses. Note that when $t_0$ is set to zero the system reverts to a simple one-mass model. Thus, except for the additional phase locking parameter $t_0$, the linear stability analysis of the system equations is identical to that for the one-mass model presented in [4, 15, 16]. The system equations are written in state space formulation as $\dot{q} = Mq$, with $q = [h, \psi, \dot{h}, \dot{\psi}]$ the state space vector, $h(t)$ the time varying part of the height $H(t)$ of the first mass or simply the displacement of the first mass, $p_m = \frac{d\psi}{dt}$ the time varying part of the mean pressure $P_m$ in the obstruction and $M$ the state space matrix.

In order to express the displacement of the second mass as a function of both the additional parameter $t_0$ and the state space variables related to the displacement of the first mass, the relationship $h(t - t_0) = f(t_0, h(t), \dot{h}(t))$ needs to be retrieved. The desired expression for the displacement of the second mass follows directly from the expansion $h(t - t_0) = h(t) - t_0\dot{h}(t)$.

As in [4, 15, 16] and accounting for $P_m(P_{up}, h(t), h(t - t_0))$ the equations describing the mechanics and acoustics of the replica are given as:

$$\begin{aligned}
&\frac{\mathrm{d}^2h(t)}{\mathrm{d}t^2} + \frac{\omega_L}{Q_L}\frac{\mathrm{d}h(t)}{\mathrm{d}t} + \frac{\omega_L^2}{2}h(t) = \frac{-1}{\mu_L}\psi, \\
&\frac{\mathrm{d}^2\psi(t)}{\mathrm{d}t^2} + \frac{\omega_d}{Q_d}\frac{\mathrm{d}\psi(t)}{\mathrm{d}t} + \omega_d^2\psi \\
&= \left(\frac{Z_d\omega_d}{Q_d}\right)\left[\frac{-\overline{H}^2\psi w^2}{\rho\overline{U}} - \frac{t_0\overline{U}\dot{h}}{\overline{H}} + \frac{\overline{U}h}{\overline{H}}\right].
\end{aligned} \tag{1}$$

The state space variable $H(x, t)$ is linearised as $H(x, t) = \overline{H} + h(t)$ with $\overline{H}$ the value at equilibrium, $\overline{U}$ denoting the mean volume velocity of the flow, $\omega_L$ the mechanical resonance frequency of the latex tubes, $Q_L$ the quality factor of the resonance $\omega_L$, $\omega_d$ the acoustical resonance frequency of the downstream waveguide, $Q_d$ the quality factor of the resonance $\omega_d$, $Z_d$ the peak value of the acoustical impedance at $\omega_d$ and $\mu_L$ the effective mass. Note that, for $t_0 = 0$, the expressions for the simple one-mass model are retrieved, as expected [4, 16]. Hence the following expression for the state space matrix $M$ is obtained, in which $\rho$=1.2 kg/m$^3$ denotes the air density and $w$=25 mm the fixed replica width:

$$M = \left[\begin{array}{cc|cc}
0 & 0 & 1 & 0 \\
0 & 0 & 0 & 1 \\
\hline
-\omega_L^2 & 0 & -\frac{\omega_L}{Q_L} & -\frac{1}{\mu_L} \\
\frac{Z_d\omega_d}{Q_d\overline{H}}(\overline{U}) & -\omega_d^2 & -\frac{t_0 Z_d\omega_d\overline{U}}{Q_d\overline{H}} & -\left(\frac{Z_d\omega_d w^2\overline{H}^2}{\rho Q_d\overline{U}}\right) - \frac{\omega_d}{Q_d}
\end{array}\right]. \tag{2}$$

The initial value $\overline{H}$ is characteristic for the geometry at equilibrium. In the case of the one-delayed-mass model, the value used is directly obtained from measurements. The mean volume airflow velocity $\overline{U}$ follows from the Bernoulli equation, corrected for viscosity by adding a Poiseuille term [22].

### 3.2. Two-mass model and linear stability analysis

The linear stability analysis of distributed two-mass models [8] is extensively discussed in [15] and details can be found there. The state space matrix $M$ for the two-mass model, accounting for flow separation and acoustical coupling, is given in equation 3. The first and second mass in the flow direction are given the subscripts 1 and 2, respectively. The subscripts $u$ and $d$ refer to the upstream and downstream parts of the replica. The vertical displacements of the masses along the z-axis are denoted $h_{1,2}$. $\overline{H}_2$ indicates the equilibrium position of the second mass and, as before, $w$ the width of the replica. The set of mechanical model parameters $(K, K_{1,2}, R, m)$ for the two-mass model includes: $K$ the spring constant, $K_{1,2}$ the coupling spring constant between the two masses, $R$ the damping constant, $m$ the mass. $F_{1,2}$ denotes the aerodynamic force transmitted to each mass. Note that the two masses $m$ and spring

constants $K$ are taken to be identical. The set of acoustical quantities $(Z_d, Q_d, \omega_d)$ is similar to that for the one-delayed-mass model and takes into account the presence of an upstream and/or downstream waveguide. The air density and volume airflow velocity are indicated as $\rho$ and $U$, respectively. As for the one-delayed-mass model, the airflow is described by the Bernoulli equation corrected for viscosity by adding a Poiseuille term [22].

Defining the state space vector as $q = [h_1,\ h_2,\ \psi_d,\ \dot{h_1},\ \dot{h_2},\ \dot{\psi_d}]^T$, the system equations can be written as $\dot{q} = Mq$ with $M$ given by:

$$M = \left[\begin{array}{cc} 0 & 0 \\ 0 & 0 \\ 0 & 0 \\ \hline -\frac{2}{m}\left(K + K_{12} - 2\frac{\partial F_1}{dH_1}\right) & \frac{2}{m}\left(K_{12} + 2\frac{\partial F_1}{dH_2}\right) \\ \frac{2}{m}\left(K_{12} + 2\frac{\partial F_2}{dH_1}\right) & -\frac{2}{m}\left(K + K_{12} - 2\frac{\partial F_2}{dH_2}\right) \\ \frac{Z_d\omega_d}{Q_d}\frac{\partial U}{\partial H_1} & \frac{Z_d\omega_d}{Q_d}\frac{\partial U}{\partial H_2} \end{array}\right.$$

$$\left.\begin{array}{c|ccc} 0 & 1 & 0 & 0 \\ 0 & 0 & 1 & 0 \\ 0 & 0 & 0 & 1 \\ \hline 0 & \frac{-2R}{m} & 0 & \frac{4}{m}\frac{\partial F_1}{\partial P_d} \\ 0 & 0 & \frac{-2R}{m} & \frac{4}{m}\frac{\partial F_2}{\partial P_d} \\ -\omega_d^2 & 0 & 0 & -\frac{\omega_d}{Q_d} + \frac{Z_d\omega_d}{Q_d}\frac{\partial U}{\partial P_d} \end{array}\right] . \quad (3)$$

In the same way as presented in [8], the mechanical parameters $K$ and $R$ are increased to $K = 4K$ and $R = R + 2\sqrt{Km/2}$, respectively, to account for non-linear behaviour when collisions occur. The criterion to detect a collision is given by $h_{1,2} < h_{crit}$, with $h_{crit}$ a constant critical height. Consequently, when collision is detected, the values of $K$ and $R$ that occur in $M$, are altered accordingly.

## 4. Experimental results and discussion

In the following section, the experimental results from the 'in-vitro' replica are discussed in order to assess the importance of firstly, the open area estimation and secondly, of the independent initial conditions of the model. Image acquisition of the open area and feature extraction is discussed in subsection 4.1. Next, subsections 4.2 and 4.3 deal with the measurement of the input parameters required for the linear stability analysis proposed in section 3. Finally, the measurements in relation to oscillation onset and offset are discussed in subsection 4.4. Different initial conditions are obtained by experimentally assessing a large range of internal pressures $P_{in}$ for three different initial geometrical configurations of the replica, i.e. firstly, no separator (0.0 mm), secondly, a separator of height 0.5 mm and thirdly, a separator of height 1.0 mm, labelled separator 0.0, 0.5 and 1.0 mm, respectively. For each configuration the influence of a downstream uniform acoustical waveguide of 50 cm length on the oscillation onset and offset is experimentally assessed. The choice of the length of the downstream waveguide of 50 cm is motivated by the common interest from both musical and speech acoustics,

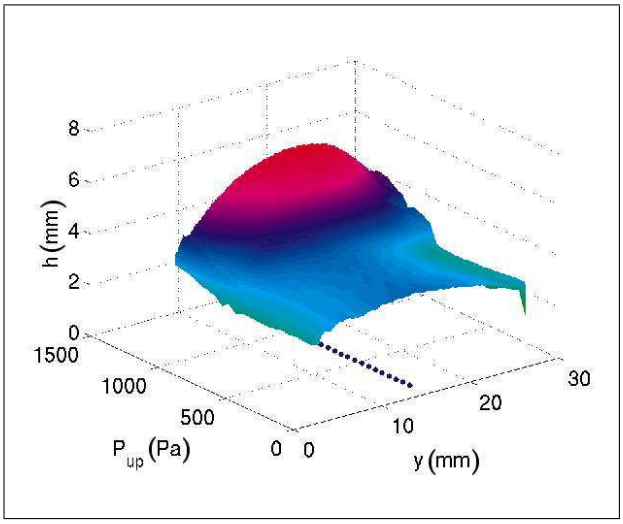


Figure 3. Exemplary aperture feature extraction $h(y, P_{up}, P_{in})$ as a function of $P_{up}$, ranging from 0 up to 1500 Pa. The dotted line indicates the centre line $y = 15$ mm for which the centre height $h_c = h(y = 15)$ is obtained.

as well as the availability of previous 'in-vitro' experimental studies [15].

### 4.1. Open area visualisation and feature extraction

Application of the image processing procedure explained in section 2.2.3 to the acquired images allows retrieval of the position of the open area in the global image. Detection of the upper and lower edges of the open area in consecutive images enables retrieval of the initial position and displacements of the latex tubes, since the open area edges coincide with the extremities of the deformable part of the latex. Consequently, consecutive registration of the changing position of both edges during the interaction with the airflow quantifies the deformation of the replica during the fluid-structure interaction. The aperture height of the open area, or the distance between the upper and lower tube edge, $h(y)$, can immediately be derived by subtraction. The value of $h(y)$ so obtained is illustrated in Figure 3 for $P_{up}$ ranging from 0 up to 1500 Pa. The dotted line $y = 15$ mm in Figure 3 indicates the centre of the replica. The height $h$ obtained for $y = 15$ mm corresponds to the centre height $h_c = h(y = 15)$, measured in previous studies using an optical laser set-up [16]. Figure 3 clearly shows that in general the height $h(y)$ is not equal to the centre height $h_c$. For example, this is the case for high values of $P_{up}$ where the centre aperture $h_c$ is almost twice the aperture value at the borders $y = 0$ and $y = 25$ mm. Consequently, in this case, a severe overestimation of the open area value $A_c = h_c w$ occurs if a rectangular open area, calculated from the measured height $h_c$ and constant width $w = 25$ mm, is assumed.

Both the geometrical area-height relationship and the two-dimensional airflow description assume a rectangular open area with constant width, in accordance with the requirements for the reduced models detailed in section 3. This assumption is currently maintained. This implies that

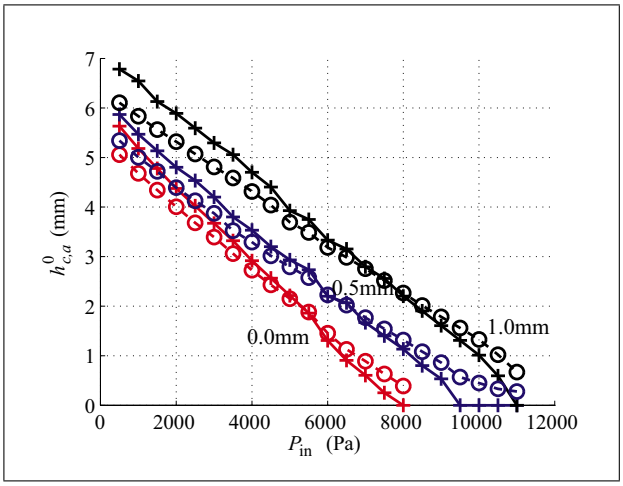


Figure 4. Initial equilibrium apertures, $h_a^0(P_{up}=0)$, derived from the total open area $h_a^0$ (markers □, ∘, △, connected with dashed lines) and at the centre $h_c^0$ (markers x, * and +, connected with full lines) for separators 1.0, 0.5 and 0.0 mm as function of $P_{in}$.

a suitable function for $h_a$ must be derived from the images in order to maintain a linear relationship between the model input aperture $h$ and the measured open area. It is therefore proposed that the aperture $h_a$ be expressed as a function of the measured open area $A_a$, as $h_a = \frac{A_a}{w}$, instead of estimating the open area value from the measured centre height $h_c$ as $h_c w = A_c$. The deduced $h_a$ values correspond to the actual measured area and hence the previous mentioned over- and under-estimation of the open area calculated from the measured centre height is avoided.

### 4.2. Equilibrium imaging and feature extraction

In order to obtain the initial position of the latex tubes at equilibrium, the open area $A_a^0$ is visualised and the aperture $h_a^0$ is extracted as discussed above in section 4.1. Here, the superscript 0 denotes the value at equilibrium i.e. in the absence of oscillations. The internal pressure $P_{in}$ is gradually increased in steps of 50 Pa from 500 Pa up to partial closure of the gap between the latex tubes, for $P_{up} = 0$; set at $P_{in} = 8000$ Pa for a gap separator of 0.0 mm and to $P_{in} = 11000$ Pa for 0.5 and 1.0 mm gap separators. It can be observed that the findings deduced for $h_a^0$ also hold for the open area $A_a^0$, since $h_a^0$ is obtained by dividing the measured $A_a^0$ by the fixed width $w$. Figure 4 summarises the initial equilibrium apertures $h_a^0$ and $h_c^0$ corresponding to $P_{up} = 0$ as a function of $P_{in}$. In the following section the symbol $h_{c,a}$ is used when this reasoning holds for both $h_c$ and $h_a$. The linear behaviour of the aperture curves, $h_{a,c}^0(P_{in}, P_{up} = 0)$, in most of the $P_{in}$ range can be seen. The overestimation of the total area derived from $h_c^0$ for low $P_{in}$ values and the underestimation for large $P_{in}$ values, is also apparent. Note that the curves for $h_c^0$ clearly show the partial closure of the replica for large $P_{in}$ values. The derived equilibrium apertures, either from the centre height or the measured open area, allow estimation of the required parameters $\overline{H}$ and $\overline{H}_2$ in the one-(delayed)-mass and two-mass models, respectively, outlined in sections 3.1 and 3.2.

Next, the mass parameter $m$ of the latex tubes is estimated from the replica's semi-cylindrical geometry and expressed as a function of the geometrical parameter $h_{c,a}^0$ as

$$m(h_{a,c}^0) = \frac{\pi D(h_{c,a}^0)^2}{2} w \rho_{wat} \quad \text{with } D = \frac{h_{tot} - h_{a,c}^0}{2}, \tag{4}$$

$h_{tot}$=0.012 m fixed by the set-up as the constant aperture in absence of latex tubes and $\rho_{wat}$=1000 kg/m$^3$ denoting the water density. The corresponding parameter $\mu_L$ is derived from the geometrical mass estimation divided by the semi-cylinder surface $\pi D(h_{c,a}^0)w$ in contact with the airflow as

$$\mu_L(h_{c,a}^0) = \frac{m}{\pi D(h_{c,a}^0)w}. \tag{5}$$

Increasing the internal pressure $P_{in}$ augments the geometrical mass estimation. Adding a separator increases the geometrical parameter $h_{a,c}^0$ and hence the estimated mass value decreases. This means that, for a larger separator, less mass is seen by the airflow and so less mass is involved in the mechanical oscillations.

### 4.3. Frequency response of the replica

The measurement of the frequency response by acoustical excitation is extensively discussed in [16] and briefly detailed in section 2.2. The repeatability of the observed mechanical responses was thoroughly checked as well as the reproducibility for all separators. For each resonance frequency $F$, the quality factor $Q$ is derived from $Q = \frac{F}{\Delta F_{-3dB}}$ with $\Delta F_{-3dB}$ the -3 dB bandwidth.

The obtained experimental parameters $F$ and $Q$ correspond to the desired quantities $\omega_L$ and $Q_L$ in the mechanical equations of the one-(delayed)-mass and two-mass model outlined in sections 3.1 and 3.2. These enable the stiffness ($K \approx m\omega_L^2$) and the damping ($R \approx m\frac{\omega_L}{Q_L}$)to be calculated. The mechanical resonance frequencies, and hence the stiffness $K$ of the replica, increase with $P_{in}$. The quality factors Q of the resonance frequencies vary between 3 and 25. A small Q value or large bandwidth corresponds to a large damping $R$ of the resonance peak and vice-versa.

### 4.4. Oscillation thresholds

The onset and offset $P_{up}$ threshold, corresponding to the minimum upstream pressure $P_{thres}$ necessary to initiate and to maintain self-sustained oscillations of the replica, as well as the associated oscillation frequency $F_0$, are experimentally assessed for different initial apertures and mechanical properties. As discussed in sections 4.2 and 4.3, the mechanical properties are varied in a controllable way by imposing different $P_{in}$, while the initial aperture is varied by mounting different separators of 0.0, 0.5 and 1.0 mm. The acoustical resonance frequency of the downstream 50 cm waveguide, $\omega_d^{50} = 170$ Hz, is generally situated between the first and second mechanical resonance

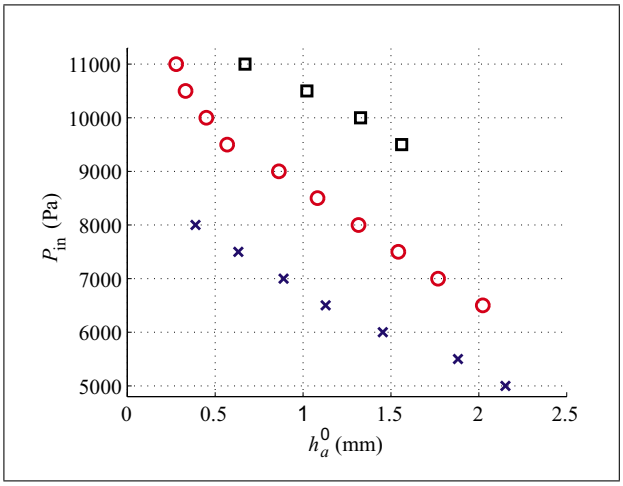


Figure 5. Part of the assessed $(P_{in}, h_a^0)$ parameter space presented in Figure 4 for which oscillations are experimentally observed in the presence of a 50 cm downstream waveguide and separators 0.0 (x), 0.5 (∘) and 1.0 mm (□).

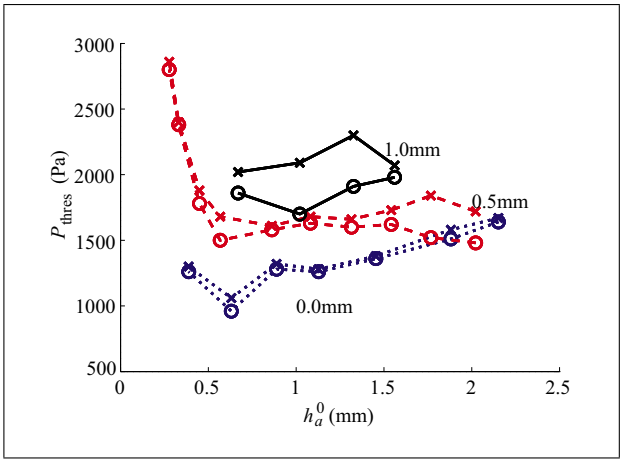


Figure 6. Measured $P_{thres}$ as a function of $h_a^0$ for a downstream waveguide of 50 cm assessed in the presence of separators of 0.0 (dotted lines), 0.5 (dashed lines) and 1.0 mm (full lines). The markers (x) and (∘) indicate values corresponding to onset and offset of vibration, respectively.

frequencies. The part of the $(P_{in}, h_a^0)$ parameter space for which self-sustained oscillations are experimentally observed is depicted in Figure 5. Compared to previous studies, for which only data for separator 0.0 mm were obtained, the explored region in the $(P_{in}, h_a^0)$ parameter space is largely extended since oscillations are observed for multiple $h_a^0$ values while $P_{in}$ remains constant. From this point of view the experimental results presented in Figure 5 are important. Moreover, since self-sustained oscillation is a non-linear phenomenon, oscillation characteristics depend on the initial conditions. Hence, the obtained data allow a more thorough experimental validation, including the influence of initial conditions, of the theoretical model performance.

Measurements of the threshold $P_{thres}$ in the upstream pressure $P_{up}$ and the associated oscillation frequencies $F_0$

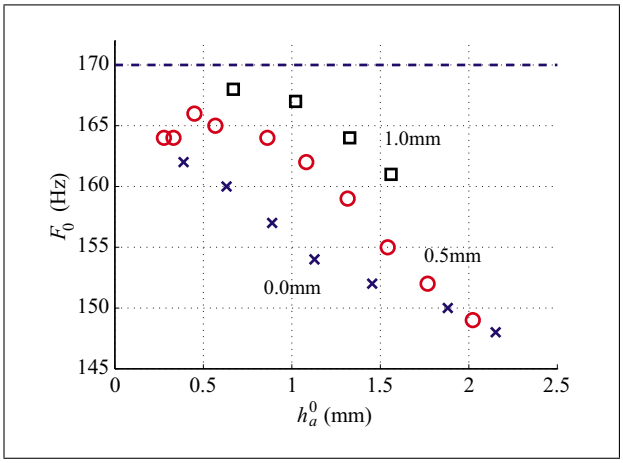


Figure 7. Measured $F_0$ as a function of $h_a^0$ for a downstream waveguide of 50 cm assessed in the presence of separators of 0.0 (x), 0.5 (∘) and 1.0 mm (□). The acoustical resonance frequency of the downstream waveguide is depicted by the horizontal dashed line.

are shown in Figures 6 and 7, respectively, as functions of $h_a^0$ for all separators. The required variation of $P_{thres}$ is easily obtained experimentally since, for example, $h_a^0 \approx 1$ mm $P_{thres}$ values are calculated for the interval of ±1000 Pa from both the onset and offset values. Oscillations are experimentally observed for initial apertures of $h_a^0 < 3$ mm, which correspond to apertures down to closure, and hence elevated internal pressures $P_{in}$. From Figure 6 a hysteresis phenomenon between onset and offset $P_{thres}$ is observed. This experimental finding is in agreement with previous studies [6]. A sudden increase in $P_{thres}$ is found for a separator of 0.5 mm for large $P_{in}$ or small $h_a^0$ values. The increase is due to a change in mechanical characteristics after partial closure of the replica, as illustrated in the parameter space depicted in Figure 4. In agreement with previous studies, Figure 7 illustrates that in case of a long downstream waveguide of 50 cm the acoustical coupling determines the oscillation frequency of the replica, since all retrieved values fall within a range of 15% below the acoustical resonance frequency of the downstream waveguide.

In the following section, modelling of the resonance characteristics $(P_{thres}, F_0)$ as a function of $(P_{in}, h_a^0)$ is assessed.

## 5. Modelling results and discussion

The physical modelling discussed in section 3 is applied to the experimental data in order to validate the model, exploiting the relationship between experimental control parameters and physical model input parameters. Firstly, an assessment is made of the use of the aperture derived from the measured open area $h_a$ instead of the measured centre height $h_c$, as the geometrical model input parameter at equilibrium (denoted $\overline{H}_{(2)}$ in the model description of section 3). Secondly, the influence of independent initial conditions, i.e. the set $(h_a^0, P_{in})$, is considered by mounting different separators while $P_{in}$ is maintained.

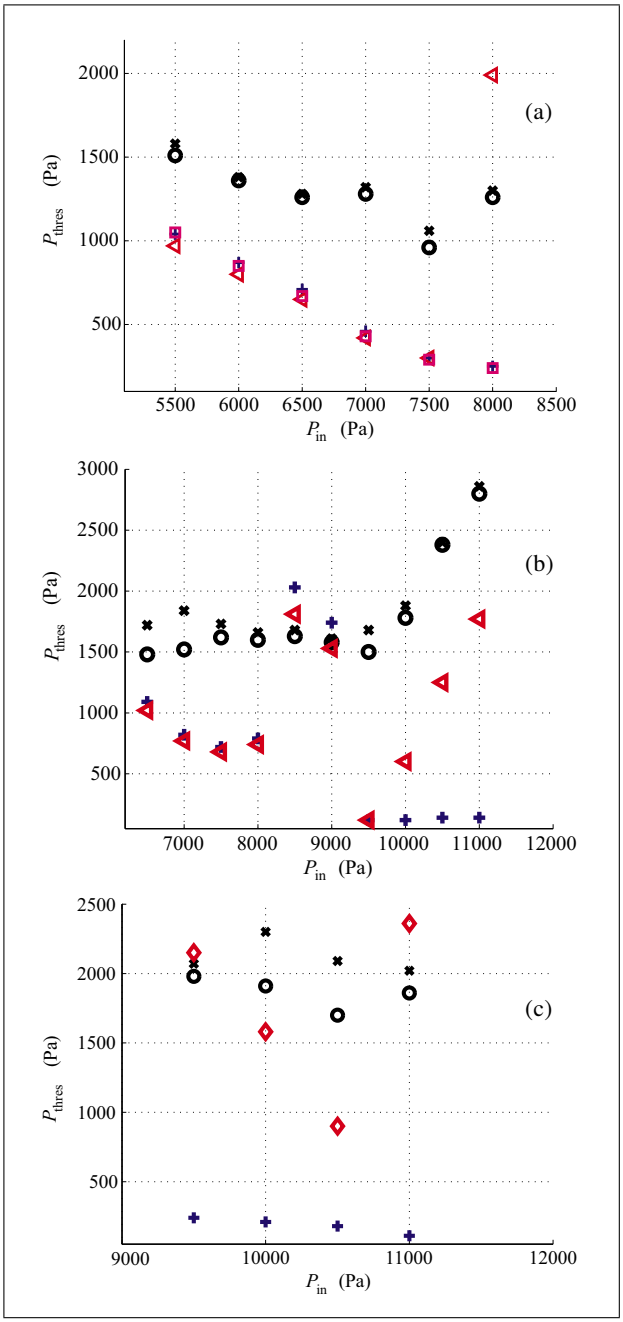


Figure 8. Experimentally observed onset (×), offset (○) and modelled $P_{thres}$ as functions of $P_{in}$, for separators (a) 0.0, (b) 0.5 and (c) 1.0 mm: (+) two-mass model with $h_{crit}$ = 0.02 mm and geometrical $h_a^0$ mass estimation, (◁) two-mass model with $h_{crit}$ = 0.5 mm and geometrical $h_a^0$ mass estimation, (□) one-mass model with $h_{crit}$ = 0.02 mm and geometrical $h_a^0$ mass estimation, (◇) two-mass model with $h_{crit}$ = 0.02 mm and mass estimated from the mechanical resonance frequency.

To each set ($h_a^0$, $P_{in}$) there corresponds a parameter set ($F, Q, m$). In practice, the $m$ parameter values are estimated from geometrical reasoning as explained in section 4.2, while the values of $F$ and $Q$ are given in Table I.

Different model results are assessed. Figure 8 illustrates some of the main points of the model validation with respect to the experimentally observed oscillation thresholds $P_{thres}$. For small internal pressures the validation of the theoretical model predictions is not possible, since the predicted thresholds exceed the maximum pressure supplied by the pressure tank. The prediction obtained using the two-mass model for $h_a^0$ and the geometrical mass parameter estimation underestimates $P_{thres}$ to a large extent ($\gg$ 10%) and $F_0$ slightly ($\leq$ 10%), as depicted in Figures 8 and 9.

The qualitative differences between the two-mass model results, obtained with either $h_a^0$ or $h_c^0$ as input parameter, are negligible up to partial closure of the replica, and this applies to $P_{thres}$ as well as $F_0$. After partial closure the differences are related to the impact of both the viscosity term in the flow description and the collision detection ($h_{crit}$=0.02 mm) applied in the mechanical descrip-

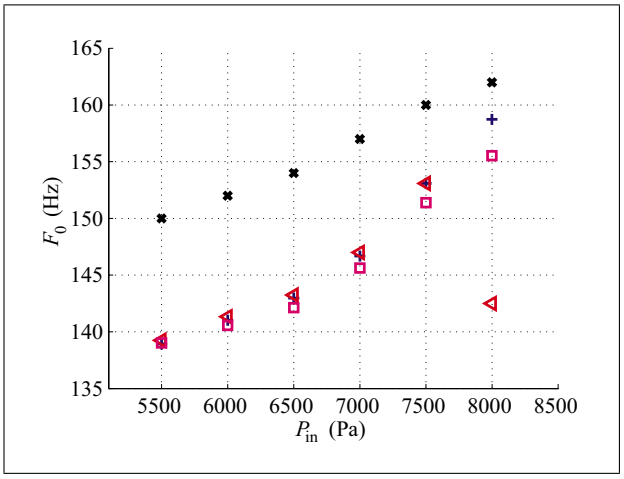


Figure 9. Experimentally observed (×) and modelled $F_0$ as functions of $P_{in}$ for separator 0.0 mm: (+) two-mass model with $h_{crit}$ = 0.02 mm and geometrical $h_a^0$ mass estimation, (◁) two-mass model with $h_{crit}$ = 0.5 mm and geometrical $h_a^0$ mass estimation, (□) one-mass model with $h_{crit}$ = 0.02 mm and geometrical $h_a^0$ mass estimation, (◇) two-mass model with $h_{crit}$ = 0.02 mm and mass estimated from the mechanical resonance frequency.

Table I. Measured mechanical frequency response parameters F and associated Q as function of $P_{in}$ (Pa) applied in the modelling.

| | 500 | 1000 | 1500 | 2000 | 2500 | 3000 |
|---|---|---|---|---|---|---|
| F (Hz) | 176 | 161 | 181 | 197 | 209 | 218 |
| Q | 8 | 12 | 15 | 15 | 17 | 17 |
| | 3500 | 4000 | 4500 | 5000 | 5500 | 6000 |
| F (Hz) | 162 | 163 | 164 | 166 | 132 | 141 |
| Q | 7 | 7 | 5 | 6 | 4 | 6 |
| $P_{in}$[Pa] | 6500 | 7000 | 7500 | 8000 | 8500 | 9000 |
| F (Hz) | 165 | 165 | 170 | 177 | 231 | 231 |
| Q | 5 | 7 | 9 | 7 | 7 | 7 |
| $P_{in}$[Pa] | 9500 | 10000 | 10500 | 11000 | | |
| F (Hz) | 108 | 109 | 110 | 111 | | |
| Q | 8 | 8 | 8 | 9 | | |

Table II. Mass estimation (g) obtained from fitting the experimental data with the two mass model for each of the separators.

| | 5000 | 5500 | 6000 | 6500 | 7000 |
|---|---|---|---|---|---|
| 0.0 mm | 0.026 | 0.034 | 0.039 | 0.055 | 0.088 |
| 0.5 mm | - | - | - | 0.028 | 0.048 |
| 1.0 mm | - | - | - | - | - |
| | 7500 | 8000 | 8500 | 9000 | 9500 |
| 0.0 mm | 0.096 | 0.270 | - | - | - |
| 0.5 mm | 0.049 | 0.053 | 0.026 | 0.037 | 1.80 |
| 1.0 mm | - | - | - | - | 0.37 |
| | 10000 | 10500 | 11000 | | |
| 0.0 mm | - | - | - | | |
| 0.5 mm | 3.20 | 8.60 | 16 | | |
| 1.0 mm | 0.60 | 0.89 | 1.8 | | |

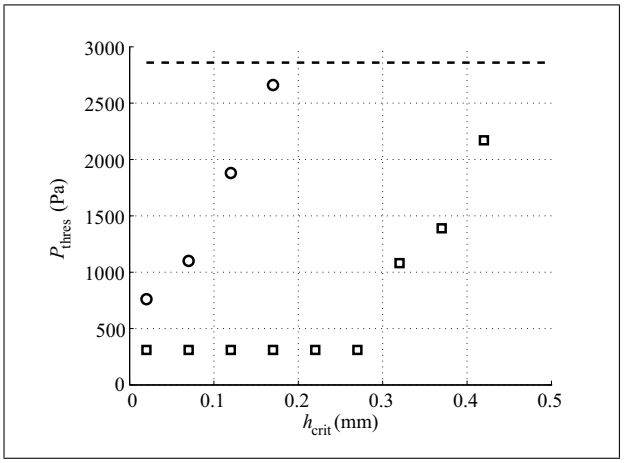


Figure 10. Influence of the aperture criterion $h_{crit}$ triggering the application of the collision model on the simulated $P_{thres}$ for features derived from $h_a$ (□) and $h_c$ (○) for separator 0.5 mm and $P_{in}$=11000 Pa. The dashed line indicates the experimentally observed $P_{thres}$ value.

tion [22]. Both phenomena become predominant for small aperture values. Such small values are attained for the centre aperture $h_c^0$ during partial closure of the latex tubes, but not for $h_a^0$, due to the remaining leaking open area related to the non-uniform closure of the tubes.

So, in general, it is found that the two-mass model with $h_a$ as input parameter presents a qualitative estimation of $P_{thres}$ and $F_0$ up to partial closure. The one-delayed-mass model predictions for $h_a^0$ leads to the same findings as obtained from the two-mass model.

The discussed predictions are obtained with the input parameters ($F$,$Q$). These are found from the measured frequency response and the geometrically estimated mass-related model parameter $m(h_a^0)$, which presents a physically meaningful upper bound for the mass parameter. Although, since the geometrical mass parameter estimation $m(h_a^0)$ cannot be experimentally validated, and since the mass parameter is seen to influence the modelled $P_{thres}$ to a large extent, alternative mass parameter estimation procedures are proposed. Firstly, the mass parameter is estimated from the mechanical resonance frequency $F$ as in [4]. The resulting mass parameter estimation $m(F)$ yields qualitatively good modelling results for separator 1.0 mm, as illustrated in Figure 8c, but not for separators 0.0 and 0.5 mm. Therefore, secondly, the mass parameter is directly derived from the mechanical equation at equilibrium. Since at equilibrium all the derivatives are zero, the mechanical part reduces to $Kh/m = f(P_{up})/m$, with $f(P_{up})$ the force exerted by the airflow. Therefore, the resulting mass parameter is not only determined by the observed geometry $h_a^0$, but also by the mechanical resonance frequency $F$ and the upstream pressure $P_{up}$, i.e. $m(h_a^0, P_{up}, F)$. This approach allows fitting of the mass parameter to exactly match the experimentally observed $P_{thres}$. The fitted parameter values obtained by applying the two-mass model for all separators are presented in Table II. As with the geometrically estimated mass, the fitted mass parameter reduces when the separator height increases for constant $P_{in}$. The influence of the mechanical frequency $F$ is evidenced by considering the evolution of the fitted mass parameter with increasing $P_{in}$. In general the fitted values again increase with $P_{in}$, corresponding to the influence of $h_a^0$ on the mass prediction. However, considering, for example, the mass evolution for separator 0.5 mm, a sudden decrease in the fitted parameter value is observed between $P_{in}$=8000 and 8500 Pa due to a jump in the resonance frequency, as can be seen in Table I. Furthermore, it can be seen that the fitted mass parameter values up to partial closure are, in general, much below the geometrically estimated values (approximately by a factor of 10). In contrast, after partial closure, the fitted values significantly exceed the geometrically estimated upper bound by a factor of 10. Therefore, after partial closure, the fitted mass values largely exceed the physical acceptable limit. This again emphasises the necessity of including an adequate collision model in the threshold predictions.

To verify the impact of the collision, the simple collision detection criterion $h_{crit}$=0.02 mm included in the two-mass model is adapted for the parameter $h_a^0$ by varying $h_{crit}$. The influence of $h_{crit}$ on $P_{thres}$ is illustrated in Figure 10 for separator 0.5 mm and $P_{in}$ = 11000 Pa. Here, the predictions are obtained using the two-mass model with either $h_a^0$ or $h_c^0$ as input parameter. The need to increase $h_{crit}$ in case of $h_a^0$ compared to $h_c^0$ is clearly illustrated. An estimation of $h_{crit}$ can be experimentally deduced by considering the remaining open area at partial closure and the resulting two-mass model outcome with $h_{crit}$=0.5 mm. The geometrical mass estimation is illustrated in Figure 8 for separators 0.0 and 0.5 mm. Because of the large influence of the collision model on the predicted $P_{thres}$, the implementation of a more advanced collision model is appropriate.

This seems particularly important in the study of brass instruments, where a player provokes initial lip closure in an attempt to attain the minimum oscillation threshold in order to play the instrument with the least effort. Re-

garding the understanding of vocal fold oscillations, the modelling of initial vocal fold apertures for similar mechanical characteristics is important in an overall model of voiced sound production, since in general the glottis is not closed at phonation onset. So a complete phonation model, which includes the phonation quantities $P_{thres}$ and $F_0$ under study, seems to require a more accurate mass prediction and even a more elaborated model approach. Furthermore, it should be noticed that a remaining open area, i.e. $h_a^0 > 0$, corresponds to the physical reality during a large portion of the glottal cycle and the constant presence of glottal leakage [23]. In addition, models expressed as a function of the open area might be interesting for studying non-parallel initial vocal fold geometries.

## 6. Conclusion

The current paper presents experimental observations with a digital camera on an improved deformable vocal fold or lip replica suitable for validating theoretical low-dimensional models. Experimental results have established the influence of independent initial conditions on the observed oscillation onset and offset pressures, as well as the oscillation frequency. In a first attempt to include the measured open area in the modelling, commonly used low order models, in which the geometrical input parameter is derived from the measured open area as an averaged aperture, are assessed. It is concluded that the models are capable of predicting the oscillation thresholds and frequencies qualitatively. Quantitative predictions remain difficult for mainly three reasons: 1) the estimation of the model parameter $m$ is critical, 2) the model itself does not accurately describe some crucial phenomena, like the contact of the lips or of the vocal folds and 3) an averaged aperture does not take account of the influence of viscosity in case of partial closure of the open area.

### Acknowledgement

Part of this work was supported by grant EMERGENCE 2004 from the Rhone-Alpes region France and as part of the France-German collaboration POPAART supported by the CNRS and the France Ministry for foreign affairs. The authors thank Prof. A. Hirschberg (Technical University Eindhoven, The Netherlands) as well as the reviewers and the associate editor for their helpful comments and suggestions. The authors wish also to thank P. Chardon (ENSERG, Grenoble, France) and Y. Garnier for their help in the design of the experimental setup.

### References

[1] F. Alipour, R. Scherer: Flow separation in a computational oscillating vocal fold model. J. Acoust. Soc. Am. **116** (2004) 1710–1719.

[2] M. de Oliveira Rosa, J. Pereira: A contribution to simulating a three-dimensional larynx model using the finite element method. J. Acoust. Soc. Am. **114** (2003) 2893–2904.

[3] E. Hunter, I. Titze, F. Alipour: A three-dimensional model of vocal fold abduction/adduction. J. Acoust. Soc. Am. **115** (2004) 1747–1759.

[4] J. Cullen, J. Gilbert, D. Campbell: Brass instruments: linear stability analysis and experiments with an artificial mouth. Acta acustica **86** (2000) 704–724.

[5] F. Avanzini, P. Alku, M. Karjalainen: One-delayed-mass model for efficient synthesis of glottal flow. Proc. Eurospeech, Aalborg, Denmark, 2001, 1–4.

[6] J. Lucero: Oscillation hysteresis in a two-mass model of the vocal folds. Journal of Sound and Vibration **282** (2005) 1247–1254.

[7] J. Jiang, Y. Zhang: Chaotic vibration induced by turbulent noise in a two-mass model of vocal folds. J. Acoust. Soc. Am. **112** (2002) 2127–2133.

[8] N. Lous, G. Hofmans, N. Veldhuis, A. Hirschberg: A symmetrical two-mass vocal-fold model coupled to vocal tract and trachea, with application to prosthesis design. Acta Acustica **84** (1998) 1135–1150.

[9] I. Titze, S. Schmidt, M. Titze: Phonation threshold pressure in a physical model of the vocal fold mucosa. J. Acoust. Soc. Am. **97** (1995) 3080–3084.

[10] R. Scherer, D. Shinwari, K. D. Witt, C. Zhang, B. Kucinschi, A. Afjeh: Intraglottal pressure distributions for a symmetric and oblique glottis with a uniform duct (L). J. Acoust. Soc. Am. **112** (2002) 1253–1256.

[11] F. Alipour, R. Scherer: Pressure and velocity profiles in a static mechanical hemilarynx model. J. Acoust. Soc. Am. **112** (2002) 2996–3003.

[12] S. Thomson, L. Mongeau, S. Frankel, J. Neubauer, D. Berry: Self-oscillating laryngeal models for vocal fold research. Proc. Flow induced vibrations, 137-142, Paris, France, 2004.

[13] C. Vilain, X. Pelorson, C. Fraysse, M. Deverge, A. Hirschberg, J. Willems: Experimental validation of a quasi-steady theory for the flow through the glottis. J. of Sound and Vibration **276** (2004) 475–490.

[14] S. Bromage, M. Campbell, J. Gilbert: Experimental investigation of the open area of the brass player's vibrating lips. Forum Acusticum, 729-734, Budapest, Hungary, 2005.

[15] I. Lopez, A. Hirschberg, A. Van Hirtum, N. Ruty, X. Pelorson: Physical modeling of buzzing lips: the effect of acoustical feedback. Acta Acustica **92** (2006) 1047–1053.

[16] N. Ruty, A. Van Hirtum, X. Pelorson, I. Lopez, A. Hirschberg: A mechanical experimental setup to simulate vocal folds vibrations. Preliminary results. ZAS papers in Linguistics **40** (2005) 161–175.

[17] S. Sastry: Nonlinear systems : analysis, stability and control. Springer-Verlag, New York, 1999.

[18] J. Gilbert, S. Bromage, M. Campbell: Influence of the open area of a player's lips on brass instrument behaviour. Forum Acusticum, 735-739, Budapest, Hungary, 2005.

[19] C. Vilain, X. Pelorson, A. Hirschberg, L. L. Marrec, W. O. Root, J. Willems: Contribution to the physical modeling of the lips. Influence of the mechanical boundary conditions. Acta Acustica **89** (2003) 882–887.

[20] R. Haralick, L. Shapiro: Computer and robot vision. Addison-Wesley Publishing Company, 1992.

[21] K. Ishizaka, J. Flanagan: Synthesis of voiced sounds from a two-mass model of the vocal cords. Bell Syst. Tech. J. **51** (1972) 1233–1267.

[22] M. Deverge, X. Pelorson, C. Vilain, P. Lagree, F. Chentouf, J. Willems, A. Hirschberg: Influence of collision on the flow through in-vitro rigid models of the vocal folds. J. Acoust. Soc. Am. **114** (2003) 1–9.

[23] B. Cranen, L. Boves: On subglottal formant analysis. J. Acoust. Soc. Am. **81** (1987) 734–746.